Journal of Electroceramics, 7, 189–195, 2001

Intrinsic Conductivity of Short Conductive Fibers in Composites by Impedance Spectroscopy

A.D. HIXSON,[1] L.Y. WOO,[1] M.A. CAMPO,[1] T.O. MASON[1] & E.J. GARBOCZI[2]
[1]*Department of Materials Science and Engineering, Northwestern University, Evanston, IL 60208, USA*
[2]*National Institute of Standards and Technology, Building Materials Division, Gaithersburg, MD 20899, USA*

Submitted July 12, 2001; Revised October 18, 2001; Accepted October 29, 2001

Abstract. Electrical property measurements (DC conductivity, impedance spectroscopy) were employed to determine the "intrinsic conductivities" of short conductive fibers in cement matrix composites. Intrinsic conductivity determines, in the dilute limit, the variation of overall conductivity (DC or AC) vs. volume fraction of fibers. Model composites consisting of steel wires (0.5 mm diameter), but with aspect ratios comparable to typical carbon or steel fibers used in cement/concrete, were shown to exhibit similar "dual-arc" impedance spectra as observed in actual composites. The results were compared with existing calculations for composites with randomly distributed right cylinders. The conductivity vs. aspect ratio behavior can be used to estimate the fiber aspect ratio in randomly distributed fiber composites.

Keywords: composites, fibers, electrical conductivity, impedance, cement

1. Introduction

Impedance spectroscopy is a widely accepted technique for investigating electrical/dielectric structure-property relationships in a variety of materials [1]. By making gain and phase angle measurements over a wide frequency range (typically MHz to Hz), real and imaginary components of the impedance (Z) can be evaluated. Plots of $-Z_{\text{imaginary}}$ vs. Z_{real}, so-called "Nyquist" plots, allow for discrete features or "arcs" to be discriminated. Recent observations of dual-arc behavior in Nyquist plots of composites with discontinuous conductive fibers [2–7] suggest that the electrical properties, both DC and AC conductivity, can be used to characterize the microstructure (fiber volume fraction, fiber aspect ratio, fiber alignment, etc.) of such composites. The approach promises to be equally valid for ceramic-matrix [2, 3] and cement/concrete matrix [4–8] composites with conductive fibers. The present work was initiated to investigate the dependence of electrical properties on the abovementioned microstructural parameters in a model composite system.

Figure 1 shows Nyquist plots at 3 days of hydration for 0.4 water-to-cement (w/c) ratio ordinary Portland cement paste (OPC) composites without and with either 1 wt% steel fibers (2 mm long, 30 μm diameter) or 1 wt% carbon fibers (18 mm initial length, 18 μm diameter). Also shown are the four-point DC resistance values, corrected for the difference in inter-electrode spacings in DC vs. AC measurements (see below). In each case, there is good agreement between the DC resistance and the cusp between the electrode arc (to the right) and the bulk features (to the left of the DC resistance). It is apparent that the presence of fibers subdivides the single bulk arc (without fibers) into two sub-arcs (with fibers). Hereafter, we refer to the cusp between the two bulk arcs as the cusp resistance, or R_{cusp}. These two values, the DC resistance (R_{DC}) and the cusp resistance (R_{cusp}), are the primary focus of the present work.

In prior work, it was demonstrated that an oxide coating on either steel or copper wires/fibers is responsible for the dual-arc behavior [4–8]. At DC or low AC frequencies, this passive oxide layer is intact and surrounds the conductive fiber with a highly resistive coating. Current flow through the surrounding matrix is essentially unperturbed by the presence of the fiber, since it acts as an insulating inclusion. As frequency

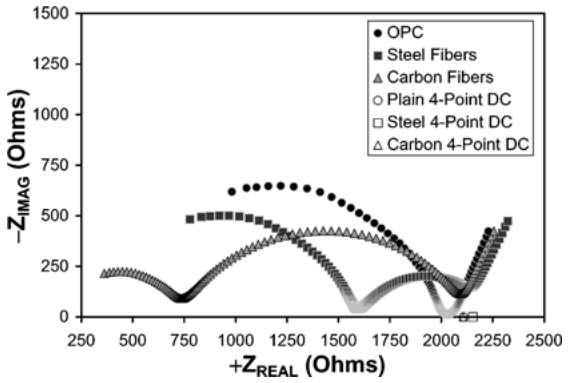

Fig. 1. Nyquist plots at 3 days of hydration for w/c = 0.4 OPC matrices without and with 1 wt% additions of either steel or carbon fibers. Four-point DC resistances are shown for comparison.

increases, however, displacement currents through the coating "capacitor" short out the film (i.e., at R_{cusp}). At this point, each fiber becomes a short-circuit or highly-conducting path through the composite. The cusp resistance reflects fiber resistance (negligible), matrix resistance due to inter-fiber current flow (as long as fiber loading is beneath the percolation threshold), and spreading resistance due to current bunching at the fiber tips. The overall resistance can be significantly reduced from R_{DC}, as is evident in Fig. 1.

Maxwell [9] first considered the classic problem of the conductivity of a dilute suspension of monosized spherical particles in which the suspended particles have a different conductivity than the suspending matrix (σ_{m}). The effective conductivity (σ)is given by:

$$\sigma/\sigma_{\text{m}} = 1 + [3(\Delta - 1)/(\Delta + 2)]\nu_{\text{f}} + O\left(\nu_{\text{f}}^2\right), \quad (1)$$

where ν_{f} is the volume fraction of the particles and Δ is the ratio of the particle conductivity to that of the matrix ($\sigma_{\text{ptcl}}/\sigma_{\text{m}}$). Although attempts have been made to calculate coefficients for the second and higher order powers of ν_{f} in the virial expansion of Eq. (1) [10–13], results are not available for complex shapes. Furthermore, the first order term typically dominates at small volume fractions of particles. Douglas and Garboczi [14] used a combination of exact analytical calculations from the literature, novel analytical calculations, and finite element analysis to compile and calculate the first order coefficients for a wide range of shapes, including right cylinders and ellipsoids of revolution, in the highly conducting and insulating limits ($\Delta \to \infty$, $\Delta \to 0$). They generalized Eq. (1) as follows:

$$\sigma/\sigma_{\text{m}} = 1 + [\sigma(\Delta)]\nu_{\text{f}} + O\left(\nu_{\text{f}}^2\right) \quad (2)$$

where $[\sigma(\Delta)]$ is the intrinsic conductivity of a particle of arbitrary shape averaged over direction (see Appendix). An accurate Padé approximation was developed to give the behavior of the entire range of Δ [15].

What is significant about Eqs. (1) and (2) is the difference in behavior between highly conducting and highly insulating particles as manifested in the first order coefficient of ν_{f}. In the case of highly conducting spheres ($\Delta = \sigma_{\text{ptcl}}/\sigma_{\text{m}} \gg 1$) Eq. (1) simplifies to:

$$\sigma/\sigma_{\text{m}} = 1 + [\sigma]_\infty \nu_{\text{f}} = 1 + 3\nu_{\text{f}} \quad (3)$$

where higher order terms have been neglected. In contrast, for highly resistive spheres ($\Delta = \sigma_{\text{p}}/\sigma_{\text{m}} \sim 0$) Eq. (1) simplifies to:

$$\sigma/\sigma_{\text{m}} = 1 + [\sigma]_0 \nu_{\text{f}} = 1 - 3/2\nu_{\text{f}} \quad (4)$$

or in terms of the "intrinsic conductivity" of Eq. (2), $[\sigma]_\infty = 3$ for infinitely conducting spheres and $[\sigma]_0 = -3/2$ for perfectly insulating spheres. Effective conductivity therefore increases with suspended particle volume fraction if the particles are conductive, but decreases if the particles are resistive. The cross-over point between increasing and decreasing behavior is when $\Delta = 1$. The premise of the present work is that impedance spectroscopy can determine both coefficients in the same suspension by turning on and off the oxide coating impedance through frequency variation.

The intrinsic conductivities of fibers are considerably different than for spheres. Taylor first calculated, using a numerical solution of exact analytical equations, the intrinsic conductivity for right cylinders [16]. Fixman [17] used a variational method to extend the calculation of the intrinsic conductivity to other aspect ratios (height-to-diameter) of infinitely conducting right cylinders. Mansfield et al. used random walk techniques to provide additional data for similar cylinders [18]. Intrinsic conductivities $[\sigma]_\infty$ can be quite large, e.g., ~100 for an aspect ratio (fiber length divided by diameter) of ~35, and increase continuously with length for a given fiber diameter. On the other hand, the intrinsic conductivity of randomly distributed, highly resistive right cylinders or prolate ellipsoids of revolution $[\sigma]_0$ is approximately –5/3 for all aspect ratios

greater than 10 [14]. Therefore, we anticipate that the DC resistance will change only slightly at small fiber volume fractions, being governed by $[\sigma]_0$, whereas the cusp resistance will change quite dramatically, being governed by $[\sigma]_\infty$.

2. Experimental Procedure

To obtain the spectra in Fig. 1, fiber-reinforced composites with 1 wt% of fibers were prepared from type I ordinary Portland cement (OPC) with a water-to-cement ratio of 0.4 by weight. Steel fibers (2 mm long, 30 μm diameter) or carbon fibers (18 mm initial length, 18 μm diameter) were dry-mixed with the cement by hand for 1 min. The water was added, followed by hand-mixing for approximately 3 min. The mixture was then blended at high speed in a commercial blender for approximately 2 min to achieve homogenization. Plain OPC specimens were similarly prepared. Specimens were cast in rectangular polycarbonate containers (25 mm $\times$ 25 mm $\times$ 100 mm) with stainless steel electrodes (20 mm $\times$ 30 mm $\times$ 0.5 mm) cast in place approximately 5 mm from each end. All samples were stored in 100% RH during curing and until measurements were made.

Most other work was carried out on model composites cast in larger (95 mm tall by 50 mm diameter) PVC molds. Again, type I OPC was mixed by hand with water at a water-to-cement ratio of 0.4, and homogenized in a commercial blender. Macro-fibers (0.5 mm diameter) made of steel were cut to three lengths (6.4 mm, 12.6 mm, and 25.3 mm) and hand-mixed into OPC paste to make up a series of specimens with 0.5 volume percent fibers. This volume fraction was chosen to ensure that the fibers would not be percolating (see below). For all types of fibers, their shape was well-modeled by a right cylinder. The samples were cured in 100% RH for 7 days, at which point the samples were subjected to impedance and four-point resistance measurements.

Aqueous electrodes were constructed for both impedance and DC studies. Specimens were mounted vertically as shown in Fig. 2, with the bottom end slightly submerged in a 1 M sodium chloride solution in which a copper mesh electrode was placed. A similar electrode arrangement was mounted at the top end of the specimen, with a sodium chloride solution reservoir and a submerged copper mesh electrode. Shielded cables connected each electrode to an impedance analyzer (Solartron 1260, Houston, TX).[1] Impedance scans were made from 11 MHz to 5 Hz at an excitation amplitude of 1 V.

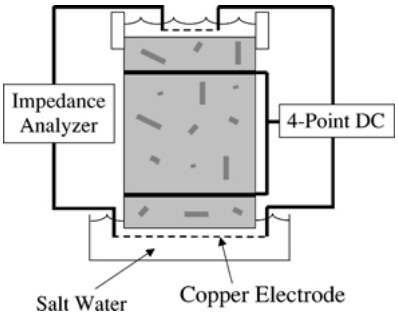

Fig. 2. Experimental set-up for impedance and 4-point DC resistance measurements.

Four-point DC measurements were made in the same apparatus, with thin steel wires wrapped tightly around the specimens at approximately 20% and 80% positions along their lengths. To facilitate electrical contact, a 2 mm-wide strip of colloidal silver paste was painted over the steel wires. These wires served as voltage leads in four-point configuration, with DC current supplied through the reservoir electrodes at the ends of the sample. Currents between $\pm$10 mA were generated by a constant current source (Keithley 220, Cleveland, OH).

3. Results and Discussion

Figure 3 shows typical impedance spectra for the macro-fiber composites investigated in the present study. The spectrum of a plain paste sample of identical age is also shown for comparison. Based upon the data in Fig. 1, we expect the plain paste to exhibit two arcs (bulk/electrode) and the composites to exhibit three arcs (bulk 1/bulk 2/electrode). These expectations were fulfilled in the case of the plain paste, but not for the composites. Instead, there is a pronounced overlap of the low frequency bulk arc with the electrode arc, to such an extent that there is no discernible cusp between the overall bulk response and the electrode response. This is most likely due to the oxide films on the steel fibers and those on the copper measurement electrodes having similar time constants. It was therefore necessary to measure the four-point DC resistances of these specimens. By correcting for the difference in geometry between four-point and two-point measurements,

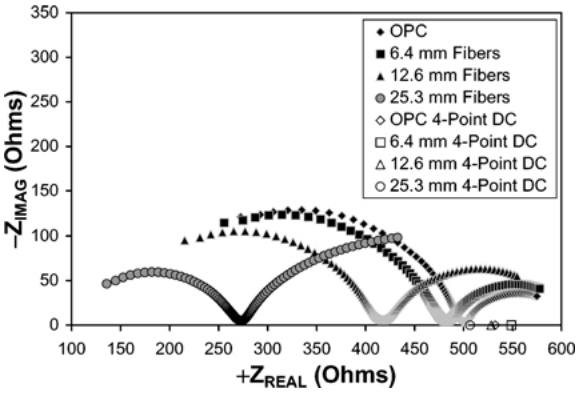

Fig. 3. Nyquist plots at 7 days of hydration for w/c ratio = 0.4 OPC matrices without and with 0.5 vol% additions of steel fibers (0.5 mm diameter) with varying lengths. Four-point DC resistances are shown for comparison.

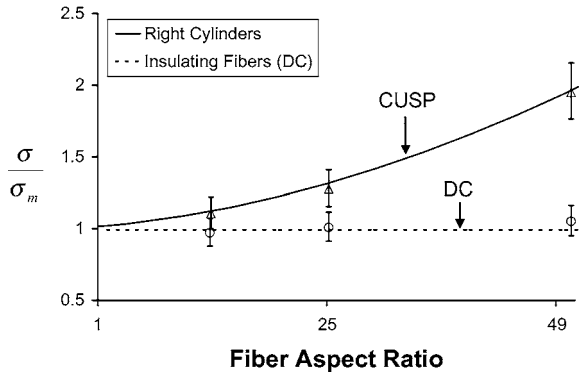

Fig. 4. Matrix(paste)-normalized DC and cusp conductivities vs. fiber aspect ratio for OPC paste (w/c ratio = 0.4) with 0.5 vol% additions of steel fibers with varying lengths. Theoretical values for right cylinders are shown for comparison.

the DC resistances could be reliably determined. These values appear as discrete points on the real axis in Fig. 3.

It is apparent from Fig. 3 that whereas the DC resistance changes very little upon fiber addition, the cusp resistance decreases markedly, and increasingly so with increasing fiber length (aspect ratio). To arrive at normalized conductivities (composite vs. paste) and intrinsic conductivities, the following procedure was followed. First, the conductivity of the plain paste (σ_p) was determined from its DC resistance ($R_{DC}(p)$) and specimen geometry using:

$$\sigma_p = l/(R_{DC}(p)A) \tag{5}$$

where l is interelectrode spacing and A is area. Similarly, the DC conductivity of each composite was determined from its DC resistance ($R_{DC}(c)$) and specimen geometry using:

$$\sigma_{DC}(c) = l/(R_{DC}(c)A) \tag{6}$$

Finally, an additional conductivity was determined from the cusp resistance (R_{cusp}) for each composite and specimen geometry using:

$$\sigma_{cusp}(c) = l/(R_{cusp}A) \tag{7}$$

It follows that if all specimens have identical geometry (l, A), the ratio of DC conductivity of a composite to that of plain cement paste is given by:

$$\sigma_{DC}(c)/\sigma_p = R_{DC}(p)/R_{DC}(c) = 1 + [\sigma]_0 \nu_f \tag{8}$$

and the ratio of the cusp conductivity of a composite to that of the plain cement paste is:

$$\sigma_{cusp}(c)/\sigma_p = R_{DC}(p)/R_{cusp}(c) = 1 + [\sigma]_\infty \nu_f \tag{9}$$

In actuality, the small sample-to-sample variations in geometry were taken into account to arrive at these conductivity ratios. Given the ±5 percent uncertainty in individual conductivity measurements (largely due to error in interelectrode spacing measurements), the ratios in Eqs. (8) and (9) will have uncertainties in the ±10 percent range.

Figure 4 shows the matrix(paste)-normalized DC and cusp conductivities vs. fiber aspect ratio. As expected, within experimental error the DC conductivities of the composites are unchanged from that of the paste. Furthermore, these conductivities do not seem to change significantly with fiber aspect ratio. This follows from Eq. (8) and setting $[\sigma]_0 = -5/3$ for insulating fibers with aspect ratios greater than 10 [14]. At a volume fraction of 0.5 percent the DC conductivity ratio is expected to be 0.992, regardless of aspect ratio. The nearly horizontal dashed line in Fig. 4 is taken from Ref. [14]. There are subtle deviations for aspect ratios less than 10 as the intrinsic conductivity deviates from $[\sigma]_0 = -5/3$ (see below).

In contrast, the matrix(paste)-normalized cusp conductivities increase dramatically with fiber aspect ratio in Fig. 4. For example, the cusp conductivity nearly doubles with the addition of 0.5 volume percent of fibers with an aspect ratio of 50.6. The upper solid line comes from theory, as described in detail below.

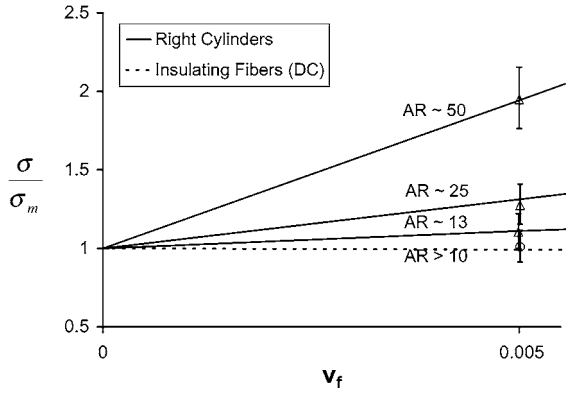

Fig. 5. Theoretical matrix(paste)-normalized conductivity vs. volume fraction for conducting right cylinders (solid lines) and for insulating prolate ellipsoids (dashed line). Also shown are experimental cusp values (triangles) and the DC value (circle) for OPC paste (w/c ratio = 0.4) with 0.5 vol% additions of steel fibers with varying aspect ratios (AR). Note that the open circle datum is actually the average of all three composites' DC values, which were virtually indistinguishable.

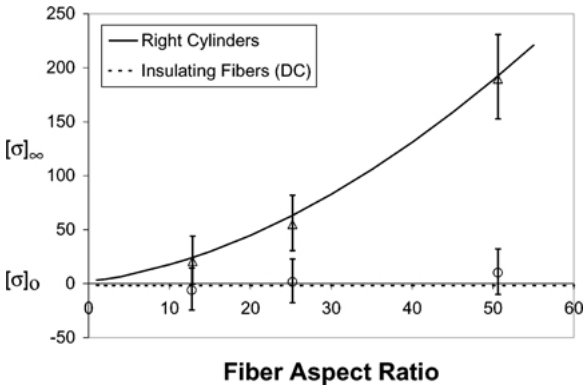

Fig. 6. Intrinsic conductivities vs. fiber aspect ratio for OPC paste (w/c ratio = 0.4) with 0.5 vol% additions of steel fibers with varying lengths. Theoretical values for right cylinders and for prolate ellipsoids (DC) are given for comparison.

In Fig. 5, the normalized conductivities are plotted vs. volume fraction. Since the DC values did not vary significantly with fiber aspect ratio, the open circle represents an average of all three composites (aspect ratios of 12.8, 25.2, and 50.6). The slope of the lower dashed line is -1.67 according to Eq. (8) and an intrinsic conductivity, $[\sigma]_0$, of $-5/3$ [14]. The upper solid lines similarly derive from theory, as described below.

Using Eqs. (8) and (9), the intrinsic conductivities can be calculated from the data in Figs. 4 or 5. The resulting values are plotted vs. fiber aspect ratio in Fig. 6. The nearly horizontal dashed line shows the expected dependence for the intrinsic conductivity of either highly resistive prolate ellipsoids of revolution or right cylinders, which are quite similar [14]. Both approach the constant value of $-5/3$ at aspect ratios greater than $\sim$10. Within experimental uncertainty, the results of the present study are in agreement with this value. There are subtle changes predicted for $[\sigma]_0$ at aspect ratios less than 10. For example, an ellipsoid of revolution becomes a sphere at an aspect ratio of one, where $[\sigma]_0$ must become $-3/2$ as in Eq. (4). The result is only slightly less, $\sim -4/3$, for a right cylinder with an aspect ratio of unity. The dashed line in Fig. 5 reflects the changes in $[\sigma]_0$ for a prolate ellipsoid of revolution as aspect ratio approaches unity.

In contrast to the highly resistive fiber intrinsic conductivity ($[\sigma]_0$), that of the conductive fibers ($[\sigma]_\infty$) rises dramatically with aspect ratio in Fig. 6. This is due to the fact that much of the matrix (paste) is now being bypassed by current flow through the fibers, which have been rendered short-circuiting by AC displacement currents through their otherwise insulating passivation layers. For comparison, we show theoretical predictions for highly conductive right cylinders [14, 16, 17] (see Appendix for the theoretical data as obtained from Fixman [17]). Within experimental uncertainty, the data in Fig. 6 agree well with the predictions for right cylinders. This suggests, at least at this volume fraction of fibers (0.5 percent), that fiber-fiber interactions are not yet significant; the composites are behaving electrically as if in the dilute range. It should be stressed that with increasing volume fraction (at fixed aspect ratio) or with increasing aspect ratio (at fixed volume fraction) fiber-fiber interactions will come into play [19]. For example, based on an excluded volume approach, the percolation threshold for fibers with an aspect ratio of 50 is approximately 1.4 volume percent [20]. Treating the fibers as prolate ellipsoids and allowing them to overlap, the estimate of the fiber volume percent at percolation is 1.5, which can be an upper bound because of the overlap criterion [21]. Ongoing studies will address this issue more closely.

The intrinsic conductivity vs. aspect ratio plot in Fig. 5 suggests a nondestructive method for establishing an otherwise unknown aspect ratio in a given composite. For example, carbon fibers are highly susceptible to breakage during the processing of fiber-reinforced cement composites. In prior work, we employed a small-scale ram extruder to produce

0.5 volume percent carbon fiber-reinforced cement composites [22]. The basic material composition by volume was: 45% cement, 1% silica fume, and 1% superplasticizer, with a water/binder ratio of 0.25. Thin specimens (4 mm thick by 25 mm wide) were found to have paste-normalized conductivities of $\sigma_{\text{cusp}}(c)/\sigma_p \sim 5.7$ (at the cusp frequency) along the extrusion direction. Thicker specimens (8 mm thick) had smaller $\sigma_{\text{cusp}}(c)/\sigma_p$ values, approximately 3.6 in the longitudinal direction. This difference is most likely attributable to differences in degree of orientation rather than to differences in fiber aspect ratio. If the thin specimen had shorter fibers due to additional breakage (smaller aspect ratio) the intrinsic conductivity should be smaller (Fig. 5) and so should be the normalized conductivity, $\sigma_{\text{cusp}}(c)/\sigma_p$. Instead, alignment of fibers can lead to an increase in intrinsic conductivity, when measured in the longitudinal direction, as much as a factor of three in fully aligned composites [14]. These results suggest that the normalized conductivity of a random arrangement of fibers must be 3.6 (as in the thick specimen) or smaller. At 0.5 volume percent of fibers, this corresponds to an intrinsic conductivity of ~500 or smaller. Using Fixman's calculation [17] of the intrinsic conductivity of long conductive fibers, this requires the aspect ratio to be ~90 or less. Since the fibers were 10 μm in diameter, this corresponds to a fiber length of ~0.9 mm. In the prior study [22], nitric acid was used to dissolve the cement paste matrix of an extruded composite, leaving the fibers behind. Optical image analysis was used to measure the length distribution of fibers. The median length was 0.75 mm, with 70 percent being between 0.35 mm and 1.5 mm. There is therefore good agreement between the electrically-derived fiber length and the median fiber length by optical microscopy. A similar approach was taken recently to compute the dielectric constant of buckminsterfullerene nanoparticles [23].

4. Conclusions

Electrical property measurements (DC conductivity, impedance spectroscopy) can be employed to determine the intrinsic conductivities of short conductive fibers in fiber-reinforced composites. The intrinsic conductivities govern the overall conductivity vs. volume fraction relationships of composites. Due to the formation of passivation layers on metallic fiber surfaces, DC (and low frequency AC) conductivity (σ) decreases only slightly with increased fiber loading, following a

$$\sigma/\sigma_m = 1 + [\sigma]_0 \nu_f = 1 - 5/3\nu_f$$

relationship, where σ_m is the matrix conductivity, ν_f is the fiber volume fraction, and $[\sigma]_0 = -5/3$ is the intrinsic conductivity, as long as the fiber aspect ratio is greater than ~10. In contrast, the cusp frequency conductivity (from the cusp in the bulk arc of impedance plots) can increase dramatically according to:

$$\sigma/\sigma_m = 1 + [\sigma]_\infty \nu_f$$

with intrinsic conductivities ($[\sigma]_\infty$) on the order of 10, 100, or more, depending on and increasing with the aspect ratio of the fibers. Experimental data for 0.5 volume percent fiber composites with different aspect ratios (12.8, 25.2, and 50.6) were found to be in good agreement with theoretical predictions for non-interacting short fibers. This agreement is expected to break down at larger fiber loadings. Furthermore, the loading at which the dilute limit is no longer valid decreases with increasing fiber aspect ratio. The experimental/theoretical intrinsic conductivity vs. aspect ratio relationship suggests that electrical properties (combined DC and impedance spectroscopy) can be used to characterize the aspect ratio in actual composites. Of course, this is only possible when accurate calculations, analytical or numerical, are available for the various intrinsic conductivities for the appropriate shapes.

Appendix

This appendix shows more details about how the intrinsic conductivities were obtained from Fixman's results [17], and gives a table of the exact values used in the figures of this paper. What Fixman obtained, using a variational method with less than 1% error, are the components of the polarizability tensor, $\alpha_{ij,}$ which in the case of a right cylinder is a diagonal second rank tensor. This accuracy was assessed by comparing to Taylor's essentially exact results [16]. Because of the symmetry of a right cylinder, two of the diagonal components are the same (transverse) and one is different (longitudinal). As the aspect ratio of the cylinder becomes large, the longitudinal component also becomes large, while the transverse components tend toward the value of 2, which is the intrinsic conductivity for a highly-conducting circle in 2-D [14].

Table 1. Longitudinal, transverse and intrinsic conductivity values for right cylinders.

Aspect ratio	Longitudinal	Transverse	Intrinsic conductivity
0.25	1.749	6.177	4.701
0.5	2.4306	4.214	3.620
1	3.858	3.169	3.399
2	7.074	2.610	4.098
4	15.061	2.314	6.563
10	4.951	2.128	17.92
20	137.08	2.064	47.069
50	589.65	2.026	197.9
100	1890.83	2.012	631.62

In Table 1 of Ref. [17], Fixman lists values of the transverse and longitudinal components of the polarizability in the conducting limit for aspect ratios of 0.25, 1, 4, 20, and 100. From Table 2 of Ref. [17], one can also extract values for aspect ratios of 10 and 50, using Eq. (4.13) in the limit $E_o \to \infty$. Table 1 lists all the values for the diagonal components, as well as the intrinsic conductivity, which is just 1/3 $(2\alpha_T + \alpha_L)$.

Note the convergence of the transverse terms to the value of 2, as the aspect ratio increases. In the limit of large aspect ratio, Landau and Lifshitz [24] have given a formula for the longitudinal component of the polarizability tensor:

$$\alpha_L = \frac{2(AR)^2}{[3\ln\{4(AR)\} - 7]} \tag{A1}$$

where AR is the aspect ratio. This agrees with Fixman's data to within 4% for the $AR = 100$ data point, and presumably gets even more accurate as the aspect ratio increases beyond this point. For lower values of the aspect ratio, this formula is increasingly inaccurate. By estimating the transverse component as 2 in the large aspect ratio limit, the formula for the intrinsic conductivity in the highly conducting, large aspect ratio limit is then

$$[\sigma]_\infty = \frac{1}{3}\left(\frac{2(AR)^2}{[3\ln\{4(AR)\} - 7]} + 4\right) \tag{A2}$$

Acknowledgments

This work was supported by the National Science Foundation under grant no. DMR-00-73197.

Note

1. Certain commercial equipment is identified in this paper in order to adequately specify the experimental procedure. In no case does such identification imply recommendation or endorsement by the National Institute of Standards and Technology, nor does it imply that the equipment used is necessarily the best available for the purpose.

References

1. J.R. Macdonald, *Impedance Spectroscopy: Emphasizing Solid Materials and Systems* (John Wiley and Sons, New York, 1987).
2. R. Gerhardt, *Proc. Ceram. Eng. Sci*., **15**, 1174 (1994).
3. C.-A. Wang, Y. Huang, Y. Li, and Z. Zhang, *J. Am. Ceram. Soc*., **83**, 2689 (2000).
4. J.M. Torrents, T.O. Mason, and E.J. Garboczi, *Cem. Concr. Res*., **30,** 585 (2000).
5. J.M. Torrents, T.O. Mason, A. Peled, S.P. Shah, and E.J. Garboczi, *J. Mat. Sci*., **36**, 4003 (2001).
6. J.M. Torrents, T.C. Easley, K.T. Faber, T.O. Mason, and S.P. Shah, *J. Am. Ceram. Soc*., **84**, 740 (2001).
7. T.O. Mason, M.A. Campo, A.D. Hixson, and L.Y. Woo, *Cem. Concr. Comp*., in press.
8. A.D. Hixson, L.Y. Woo, M.A. Campo, and T.O. Mason, *Cem. Concr. Res*., submitted.
9. J.C. Maxwell, *Treatise on Electricity and Magnetism* (Dover, NY, 1954).
10. D.J. Bergman, *Phys. Rev*., **9**, 377 (1978).
11. A.S. Sangani, *Soc. Ind. Appl. Math., J. Appl. Math*, **50**, 64 (1990).
12. H.B. Levine and D.A. McQuarrie, *J. Chem. Phys*., **49**, 4181 (1968).
13. D.J. Jeffrey, *Proc. Royal Soc. London A*, **335**, 355 (1973).
14. J.F. Douglas and E.J. Garboczi, in *Advances in Chemical Physics Vol. XCI*, edited by I. Prigogine and S.A. Rice (John Wiley & Sons, 1995).
15. E.J. Garboczi and J.F. Douglas, *Phys. Rev. E*, **53**, 6169 (1996).
16. T.T. Taylor, *J. Res. NBS*, **64**, 135 (1960).
17. M. Fixman, *J. Chem. Phys*., **75**, 4040 (1981).
18. M.L. Mansfield, J.F. Douglas, and E.J. Garboczi, *Phys. Rev. E*, **64**, 61401 (2001).
19. D.S. McLachlan, M. Blaszkiewicz, and R.E. Newnham, *J. Am. Ceram. Soc*., **73**, 2187 (1990).
20. I. Balberg, C.H. Anderson, S. Alexander, and N. Wagner, *Phys. Rev. B*, **7**, 3933 (1984).
21. E.J. Garboczi, K.A. Snyder, J.F. Douglas, and M.F. Thorpe, *Phys. Rev.* E, **52**, 819 (1995).
22. A. Peled, J.M. Torrents, T.O. Mason, S.P. Shah, and E.J. Garboczi, *ACI Mater.* J., **98**, 313 (2001).
23. C.R. Snyder and J.F. Douglas, *J. Phys. Chem.* B, **104**, 11058 (2000).
24. L.D. Landau and E.M. Lifshitz, *Electrodynamics of Continuous Media* (Addison-Wesley, Reading, MA, 1960).